Low-excitation transport and separation of high-mass-ratio mixed-species ion chains

F. Lancellotti [1,*] S. Welte [1,†] M. Simoni [1] C. Mordini [1] T. Behrle,[1] B. de Neeve [1] M. Marinelli [1,‡]
V. Negnevitsky,[1,§] and J. P. Home [1,2,‖]

[1]*Institute for Quantum Electronics, ETH Zürich, Otto-Stern-Weg 1, 8093 Zürich, Switzerland*
[2]*Quantum Center, ETH Zürich, 8093 Zürich, Switzerland*

We demonstrate low-excitation transport and separation of two-ion crystals consisting of one ^{9}Be$^+$ and one ^{40}Ca$^+$ ion, with a high mass ratio of 4.4. The full separation involves transport of the mixed-species chain, splitting each ion into separate potential wells, and then transport of each ion prior to detection. We find the high mass ratio makes the protocol sensitive to mode crossings between axial and radial modes, as well as to uncontrolled radial electric fields that induce mass-dependent twists of the ion chain, which initially gave excitations $\bar{n} \gg 10$. By controlling these stages, we achieve excitation as low as $\bar{n} = 1.40 \pm 0.08$ phonons for the calcium ion and $\bar{n} = 1.44 \pm 0.09$ phonons for the beryllium ion. Separation and transport of mixed-species chains are key elements of the quantum charge-coupled device architecture and may also be applicable to quantum-logic-based spectroscopy of exotic species.

Trapped ions are among the leading candidates for quantum computing, based on the high quality of control that is demonstrated and long coherence times [1,2]. A primary challenge remains to scale to sizes that are suitable for large-scale error correction. The quantum charge-coupled device (QCCD) [3,4] is a promising candidate architecture for this scaling. A QCCD chip employs multiple separate zones to perform specialized tasks such as quantum logic operations, storage of quantum memories, and qubit detection and reset. Ion transport and separation are used to connect separate zones, thus making them necessary ingredients to perform large-scale operations [5]. The QCCD architecture places high demands on the quality of shuttling and separation operations, which, if performed imperfectly, cause motional excitation, degrading the performance of subsequent quantum gates [6]. Such excitation can be mitigated by co-trapping a second ion species and using it to re-cool the ions [7,8]. The spectral isolation of the two species ensures that no cooling light impacts the stored qubit [9]. However, re-cooling is relatively slow and it is desirable to reduce the excitation during transport and separation operations—indeed, re-cooling has been the dominant timescale in several prominent demonstrations of the QCCD architecture [10–13].

*Contact author: flancell@phys.ethz.ch
†Contact author: weltes@phys.ethz.ch
‡Present address: JILA, Boulder, Colorado, USA.
§Present address: Oxford Ionics, Oxford OX5 1PF, United Kingdom.
‖Contact author: jhome@phys.ethz.ch

Although primarily considered here in the context of the QCCD approach and quantum computing, the control of mixed species is also important for spectroscopy, where a control ion is manipulated and cooled by laser light and co-trapped with a spectroscopy species of interest [14–16]. For spectroscopy species which are challenging to prepare or maintain, transport and separation may facilitate control. An explicit example is the use of transport and separation as part of sympathetic cooling protocols for a single (anti)proton co-trapped with a single beryllium ion [17].

Transport and separation tasks have been extensively investigated using single-species ion chains [1,18–27], with low excitation achieved over a wide range of parameters. When a second ion species of a different mass is introduced [28–32], the mass-dependent pseudopotential from the radio-frequency trapping fields introduces extra control challenges. The relative participation of each species to the radial normal modes of motion can be highly unbalanced, and different radial modes have very different frequencies [33]. In addition, stray radial electric fields displace the ions by different amounts, twisting the ion chain relative to the trap axis and changing the direction along which normal modes are defined. While these effects are present whenever two different mass ions are used, they are exacerbated by the presence of a high mass ratio.

In this Letter, we demonstrate low-excitation transport and separation of a two-ion crystal composed of one ^{9}Be$^+$ and one ^{40}Ca$^+$ ion. We identify and investigate several factors inhibiting performance, such as the presence of stray electric fields and the coupling of axial and radial modes. These are mitigated through multiposition stray electric field compensation, the addition of adjustment quadrupole terms in the potential to control mode crossings, and variation of the timescales of dynamic control. A tailored combination of these measures reduces the axial excitation of separated ions to a mean phonon number $\bar{n} < 1.85$ with separation timescales of 2.5 ms.

FIG. 1. Spatial and temporal schematic of the experiment. One row of segmented DC trap electrodes is shown in yellow. Laser beams for both species are directed through the detection zone. Single ^{9}Be$^+$ and ^{40}Ca$^+$ ions are shown as blue and red icons, respectively. The positions of the ions at different steps of the experimental protocol are indicated.

We use a segmented three-dimensional ion trap [34,35] with multiple trap electrodes to which dynamic voltages are applied in the transport and separation protocol. Figure 1 shows a sketch of the relevant electrodes as well as the experimental sequence. The protocol starts with a transport sequence T1 moving the two-ion crystal over a distance of 442.5 μm from the detection zone to the separation zone. The latter zone features narrow electrodes for generating strong higher-order potentials. We then run a separation sequence S1, which evolves the trapping potential from a single-well to a double-well configuration. It involves the use of a time-varying axial potential of the form $\Phi(z, t) = a(t)z^2 + b(t)z^4$, where z is the coordinate of the axial direction. We first ramp up the applied voltages to achieve the highest possible positive axial quartic term, then reduce the quadratic component from a positive value to a negative one until the ions are split and located in a double well [36]. The frequency of the lowest-frequency axial mode of the mixed-species Be-Ca crystal reaches its minimum when $a(t) \simeq 0$, i.e., when the potential is purely quartic—we refer to this, in what follows, as the critical point. At this point, the simulated mode frequencies are $f_{Z1} = 0.23$ MHz, $f_{Z2} = 1.05$ MHz, $f_{Y2} = 2.1$ MHz, $f_{X2} = 3.6$ MHz, $f_{Y1} = 12.79$ MHz, and $f_{X1} = 14.29$ MHz, where Z1/Z2, Y1/Y2, and X1/X2 are the axial and the two radial in-phase/out-of-phase modes, respectively [9]. Afterward, the two harmonic wells containing one ion each are independently controlled and moved apart to a distance of 865 μm, bringing one back to the detection zone while the second is moved to storage zone 1. After state diagnosis of ion 1, we perform a third parallel transport waveform (PT) which moves both potential wells such that ion 2 is brought to the detection zone, after which we perform a state diagnosis on this ion.

Prior to each run of the experiment, we deterministically initialize the ions in the order Be-Ca (^{9}Be$^+$ left, ^{40}Ca$^+$ right)

using established reordering techniques [33]. The ion crystal is laser cooled by applying Doppler cooling and EIT cooling [37] of all vibrational modes. The EIT cooling detuning is set to optimize cooling of the Y2 mode and also cools the X2 mode [38], resulting in mean occupancies $\bar{n}_{Y2} = 0.14 \pm 0.06$ and $\bar{n}_{X2} = 0.36 \pm 0.07$. The X1 and Y1 modes have higher frequencies and are Doppler cooled to $\bar{n} \sim 1$ using beryllium light prior to each sequence. For transport and separation, we focus on the axial modes since these have participation ratios suitable for multiqubit gates and sympathetic cooling [12,39]. Following Doppler and EIT cooling, we therefore sideband cool both the axial Z1 and Z2 modes close to the ground state, resulting in occupations of $\bar{n}_{Z1} = 0.03 \pm 0.02$, $\bar{n}_{Z2} = 0.01 \pm 0.02$.

Transport and separation waveforms that were previously developed [40] allow us to routinely perform separation of single-species chains of two ^{9}Be$^+$ or two ^{40}Ca$^+$ ions with an excitation close to $\Delta\bar{n}_{Be} < 0.8$ and $\Delta\bar{n}_{Ca} < 2.3$ phonons for the single-ion axial vibrational modes, respectively (example measurements are given in the Supplemental Material (SM) [35]). However, the direct use of the same transport and separation waveforms for the mixed-species chain produced large excitation of the axial modes with $\bar{n} \gg 10$ phonons, which was so severe that unwanted reordering of the crystal occurred even during the initial transport segment. A first correction step is to compensate for uncontrolled electric fields radially displacing the ions in a mass-dependent manner [33]. The primary excitations are mitigated by adding compensation potentials for stray electric fields at 11 locations along the trap axis during transport, and at 12 points in the separation zone throughout the separation waveform. Each of these is calibrated to a level of 2 V/m. This compensation allows us to reduce the crystal excitation to a level where no reordering occurs during T1, and where diagnostics based on sideband spectroscopy can be used to optimize further. Our approach is to run the sequence up to a point of interest and then reverse it after a short delay, after which the phonon population is characterized. Figure 2 shows the measured phonon occupancies of Z1 and Z2 throughout the separation sequence S1, together with the simulated frequencies of Z1, Z2, Y2, and X2 and measured frequencies of Z1 and Y2 for some relevant points. The total duration of the S1 waveform in this example is 823 μs, which was the timescale used for our initial diagnostics. The data points at negative times show the contribution of the transport waveform T1, which results in mode occupations of $\bar{n}_{Z1} \simeq 1.17 \pm 0.11$ and $\bar{n}_{Z2} \simeq 0.18 \pm 0.09$ quanta after this part of the protocol. We maintain the Y2 mode at 230 kHz lower than the Z1 mode throughout T1, and additionally maximize the frequencies of both modes to reduce heating rates.

Due to stray electric fields along the axis, applying a predesigned waveform for S1 does not necessarily end up with the ions in separate potential wells. Thus we first calibrate the stray field by scanning an additional axial field and observing the transition in populations of the final wells between two ions in the left well, one in each well, and two in the right well. For ion separation, we then proceed to use a calibrated value in the middle of the range, which results in one ion in each well. We observe daily fluctuations of this parameter of about 1 V/m, which do not significantly affect the performance. Recalibration is only necessary on a
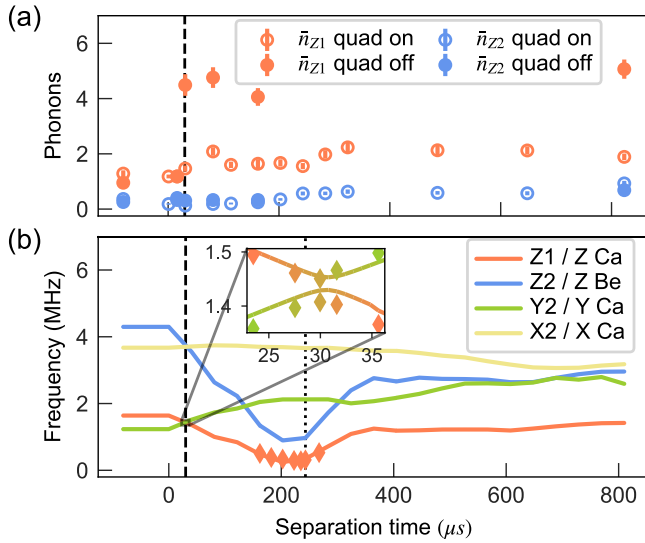
FIG. 2. (a) Time-resolved measurement of the axial phonon populations after partially running the separation sequence forward and backwards. $t = 0$ indicates the start of the separation segment, with negative times belonging to the transport waveform. (b) Simulated (solid lines) and measured (diamond points) mode frequencies of the lowest four modes throughout the waveform. Uncertainties on the measured data points are smaller than the marker size. The position of the Z1/Y2 mode crossing at 30 µs is indicated by the vertical black dashed line. After the vertical dotted line at 243 µs, the ion separation is greater than 29 µm and we consider the normal modes to be uncoupled. Inset: Measurements and simulations close to the avoided crossing between Z1 and Y2. The color change indicates the transition between the two modes.

timescale of weeks. The temperatures measured after such a calibration are shown in Fig. 2 for the separation waveform S1. We observe a significant excitation in the Z1 mode occurring at 30 µs, which corresponds in the simulation to a frequency crossing of the Z1 mode with the Y2 mode, highlighted with a black dashed line. Under the conditions of our transport waveform, this is inevitable in separation since the axial curvature is significantly reduced. In our setup, the Y2 mode has a high heating rate of ∼3000 phonons/s and thus, despite being initially cooled down close to the motional ground state, it gains an excitation of ∼4 phonons by the time the crossing point is reached. The excitation of Z1 then results from the injection of radial phonons due to a coupling between the modes close to the degeneracy point, an effect which has previously been observed in junction transport with a single ion [41]. Measurements of the mode frequencies around the crossing point [shown in the inset of Fig. 2(b)] confirm the presence of an avoided crossing with a minimum mode separation, $\Delta/(2\pi) \simeq 23$ kHz. The components of the Hessian relevant to the two modes can be described as $-\frac{\hbar\Delta}{2}\hat{\sigma}_x - \frac{\hbar\varepsilon(t)}{2}\hat{\sigma}_z$, where σ_x and σ_z are the Pauli matrices and $\varepsilon(t)$ is the mode separation of the uncoupled modes. We can use the Landau-Zener-Stückelberg–Majorana formula [42] to estimate that the probability that the system will undergo a diabatic transition when evolving through the avoided crossing is $P_D = \exp\{-\Delta^2/[4\,|\partial/\partial t(f_{Z1} - f_{Y2})|]\}$. Using the measured Δ and our characteristic protocol speed, we obtain $P_D = 0.7$. We note that to reduce the exchange of phonons between
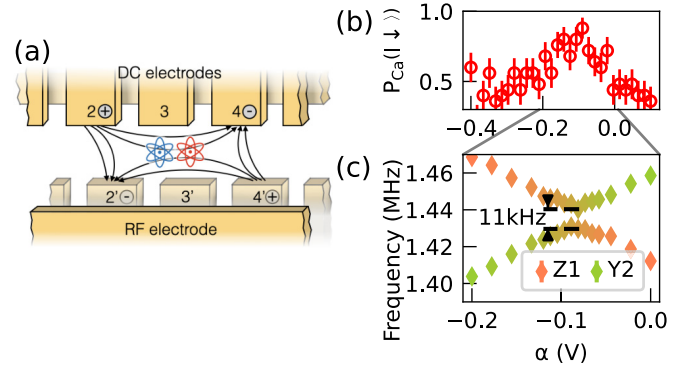
FIG. 3. Application of a quadrupole potential. (a) Schematic showing the signs of the shifts to the electrode voltages used to generate the quadrupole potential. (b) Calibration of the quadrupole scaling factor α for T1-S1. The measured spin population is a proxy for mode excitation for which a high value indicates low excitation. (c) Measurement of the Z1/Y2 mode frequencies as a function of α close to the avoided mode crossing.

the modes, the probability of a diabatic transition has to be maximized.

In the single-species case, an off-diagonal coupling term in the Hessian requires the presence of a tilted electric quadrupole, while for a mixed-species chain, such terms can also occur due to a radial electric field, which tilts the ion chain and changes the normal mode expansion along the trap axis. Such a radial field is minimized via our stray field compensation. To further suppress the off-diagonal terms, we add to $S1(t)$ a quadrupole potential $\alpha Q(t)$ using an electrode configuration illustrated in Fig. 3(a), where $Q(t)$ is a dimensionless quadrupole term and α is the scaling factor. We empirically scan α to minimize the excitation of the axial mode of $^{40}Ca^+$ at the end of the separation. Figure 3 shows results of such a calibration along with the measured trap frequencies. We observe that the minimum mode separation close to the avoided crossing point is reduced to $\simeq 11$ kHz, which corresponds to $P_D = 0.99$. For the reverse waveform, we recalibrate α by minimizing the excitation of Z1. The mode excitation of Z1 observed after passing forward and backward through the avoided crossing is reduced from 4.29 ± 0.31 quanta to 1.44 ± 0.1 quanta. For mode Z2, we notice no appreciable increase of phonons after the avoided crossings with Y2 and X2 independent of the value of α. We attribute this to the fact that the Y2 and X2 modes are strongly dominated by Ca, which in Z2 has a low participation ratio.

For transport and splitting operations performed on longer ion chains, the mode trajectories exhibit a large number of crossings. Therefore, creating crossing-free waveforms becomes increasingly hard, justifying the need for the techniques developed above. In our particular case, the small size of the ion crystal allows us to generate new transport and separation waveforms T2 and S2, which avoid mode degeneracies by keeping $f_{Y2} > f_{Z1} + 380$ kHz at all times—these produced similar results to T1-S1 with an optimized quadrupole potential.

The amount of time spent crossing the critical point also strongly affects mode excitation, due to the scaling of the heating rate $\dot{\bar{n}}$ with the trapping frequency. In a
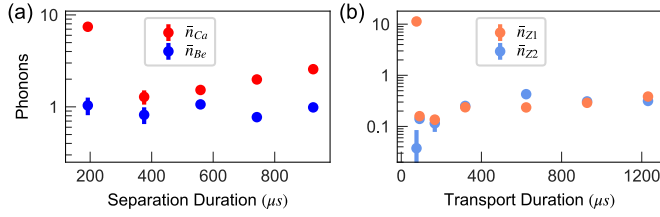
FIG. 4. (a) Excitation of axial modes after T2-S2-PT scanning the total time of S2. (b) Excitation of axial modes after the transport protocol T2-T2^{-1}. Excitation is plotted as a function of the total protocol time.

characterization measurement with one ^{40}Ca$^+$ ion, we measure this scaling for the axial mode in the detection zone and find $\dot{\bar{n}} \propto 1/f_Z^{5.8}$—we suspect this is due to increased technical noise leaking past our filters at low frequencies. Using this value, we estimate the heating rate of mode Z1 at the measured critical point frequency of 284 kHz to be 2600 quanta/s. Therefore, we aim to minimize the time spent at the critical point. A contrasting requirement is the desire to satisfy the adiabatic condition $\delta = |\frac{1}{2\pi f^2}\frac{df}{dt}| \ll 1$ throughout transport and separation to avoid coherent excitation of the ion chain [20,22,43]. As a result, we optimize the speed at which we run the separation sequence T2-S2-PT; results for the S2 segment are shown in Fig. 4(a). We observe optimal performance at a duration of 375 µs ($\delta \sim 0.015$). At shorter timescales ($\delta \sim 0.03$), we notice that the motional populations show a combination of coherent and thermal fractions, which signifies nonadiabatic excitation [20]. Scanning the timescales of the transport segments T2-T2^{-1} produced the results shown in Fig. 4(b), with a minimum transport time for the 442 µm distance of 46 µs. This corresponds to an average velocity of 9.7 m/s without diabatic excitation.

A summary of the performance of all waveforms is given in Table I, including results of separation waveforms run in one direction only, as well as forward and back sequences. We observe that the additional quadrupole allows the T1-S1 sequence to achieve similar performance to T2-S2, while the

TABLE I. Mean phonon number in the axial modes of motion for different transport/separation sequences. The upper four are for forward and back operation, probing mode Z1 using ^{40}Ca$^+$ sidebands and mode Z2 using ^{9}Be$^+$. The lower two are mean axial excitations of the calcium and beryllium ions, with the latter measured after the PT segment, which has a duration of 1.1 ms and results in excitation of 0.15 ± 0.02 quanta. The sequence duration is the time for running the full waveform sequence that is listed.

Sequence	Duration	$\bar{n}_{Z1}$	$\bar{n}_{Z2}$
T1-T1^{-1}	1.4 ms	0.82 ± 0.08	0.36 ± 0.07
T2-T2^{-1}	1.34 ms	0.46 ± 0.03	0.59 ± 0.07
T1-S1-S1^{-1}-T1^{-1}	3.2 ms	2.26 ± 0.23	0.98 ± 0.11
T2-S2-S2^{-1}-T2^{-1}	2.8 ms	3.01 ± 0.2	1.12 ± 0.13
Sequence	Duration	$\bar{n}_{Ca}$	$\bar{n}_{Be}$
T1-S1-PT	2.7 ms	1.85 ± 0.15	0.79 ± 0.09
T2-S2-PT	2.5 ms	1.40 ± 0.08	1.44 ± 0.09

lowest excitations observed are close to 1.5 quanta for ^{40}Ca$^+$ and 1 quantum for ^{9}Be$^+$. The sequence T2-S2-S2^{-1}-T2^{-1} shows an excitation that is higher than the one-directional T2-S2-PT for ^{40}Ca$^+$, with the Z1 mode being heated the most, as would be expected given that this low-frequency mode would be most affected by heating.

We also performed separation experiments with the reverse ion order, Ca-Be. Measured excitations showed no substantial difference after T2-T2^{-1}, but higher final excitations for ^{40}Ca$^+$ were observed after the separation sequence T2-S2-PT. Measurements of the heating rates of modes close to the critical point revealed much higher values for Ca-Be vs Be-Ca, for reasons which we do not understand (these measurements are presented in the SM [35]).

The demonstrated multispecies transport and separation provides a starting point for protocols using more extensive ion arrays. As a first probe of this, we apply the waveforms used for two-ion separation to Ca-Be-Ca, Be-Ca-Be, and Ca-Be-Ca-Be crystals [35]. While we do not investigate final temperatures for these larger crystals using sideband spectroscopy, we observe that the separation and recombination protocol causes no loss of fluorescence for Ca-Be-Ca, compatible with low motional excitation, and only a small loss for the other configurations. For all crystals, the ion order is maintained. The demonstrated low-excitation splitting could be sped up and the heating reduced by engineering nonadiabatic operations [20,22,43]. By focusing on the control of trapping fields, our methods are independent of the employed species or trap design that is involved. They can be readily applied to reduce the required cooling time in other QCCD experiments with different mass ratios [32,44]. In quantum logic spectroscopy protocols, where the mass ratios can be large, the developed techniques are expected to play an even more significant role. As an example, in [17], the spectroscopy signal degrades with a higher antiproton temperature, which is affected by imperfect transport and separation operations. Due to the large mass ratio, our techniques could provide a way to keep the temperature low and thereby reduce measurement uncertainties.

F.L., S.W., and M.S. performed the mixed-species experiments, while the single-species results were obtained by F.L., T.B., M.M., and V.N., with experimental support by B.N. Waveform generation was performed by C.M., V.N., and F.L. Data analysis and theoretical understanding of the results were developed by F.L., M.S., S.W., C.M., and J.H. The Letter was written by S.W., F.L., M.S., C.M., and J.H. with input from all authors.

[1] C. R. Clark, C. D. Herold, J. T. Merrill, H. N. Tinkey, W. Rellergert, R. Clark, R. Brown, W. D. Robertson, C. Volin, K. Maller, C. Shappert, B. J. McMahon, B. C. Sawyer, and K. R. Brown, Characterization of fast ion transport via position-dependent optical deshelving, Phys. Rev. A **107**, 043119 (2023).

[2] P. Wang, C.-Y. Luan, M. Qiao, M. Um, J. Zhang, Y. Wang, X. Yuan, M. Gu, J. Zhang, and K. Kim, Single ion qubit with estimated coherence time exceeding one hour, Nat. Commun. **12**, 233 (2021).

[3] D. J. Wineland, C. Monroe, W. M. Itano, D. Leibfried, B. E. King, and D. M. Meekhof, Experimental issues in coherent quantum-state manipulation of trapped atomic ions, J. Res. Natl. Inst. Stand. Technol. **103**, 259 (1998).

[4] D. Kielpinski, C. Monroe, and D. J. Wineland, Architecture for a large-scale ion-trap quantum computer, Nature (London) **417**, 709 (2002).

[5] C. D. Bruzewicz, J. Chiaverini, R. McConnell, and J. M. Sage, Trapped-ion quantum computing: Progress and challenges, Appl. Phys. Rev. **6**, 021314 (2019).

[6] V. Kaushal, B. Lekitsch, A. Stahl, J. Hilder, D. Pijn, C. Schmiegelow, A. Bermudez, M. Müller, F. Schmidt-Kaler, and U. Poschinger, Shuttling-based trapped-ion quantum information processing, AVS Quantum Sci. **2**, 014101 (2020).

[7] H. Häffner, C. F. Roos, and R. Blatt, Quantum computing with trapped ions, Phys. Rep. **469**, 155 (2008).

[8] L. Schmöger, O. Versolato, M. Schwarz, M. Kohnen, A. Windberger, B. Piest, S. Feuchtenbeiner, J. Pedregosa-Gutierrez, T. Leopold, P. Micke, A. Hansen, T. Baumann, M. Drewsen, J. Ullrich, P. O. Schmidt, and J. R. C. López-Urrutia, Coulomb crystallization of highly charged ions, Science **347**, 1233 (2015).

[9] M. D. Barrett, B. DeMarco, T. Schaetz, V. Meyer, D. Leibfried, J. Britton, J. Chiaverini, W. M. Itano, B. Jelenković, J. D. Jost, C. Langer, T. Rosenband, and D. J. Wineland, Sympathetic cooling of $^9Be^+$ and $^{24}Mg^+$ for quantum logic, Phys. Rev. A **68**, 042302 (2003).

[10] J. P. Home, D. Hanneke, J. D. Jost, J. M. Amini, D. Leibfried, and D. J. Wineland, Complete methods set for scalable ion trap quantum information processing, Science **325**, 1227 (2009).

[11] Y. Wan, D. Kienzler, S. D. Erickson, K. H. Mayer, T. R. Tan, J. J. Wu, H. M. Vasconcelos, S. Glancy, E. Knill, D. J. Wineland, A. C. Wilson, and D. Leibfried, Quantum gate teleportation between separated qubits in a trapped-ion processor, Science **364**, 875 (2019).

[12] J. M. Pino, J. M. Dreiling, C. Figgatt, J. P. Gaebler, S. A. Moses, M. Allman, C. Baldwin, M. Foss-Feig, D. Hayes, K. Mayer *et al.*, Demonstration of the trapped-ion quantum CCD computer architecture, Nature (London) **592**, 209 (2021).

[13] C. Ryan-Anderson, J. G. Bohnet, K. Lee, D. Gresh, A. Hankin, J. P. Gaebler, D. Francois, A. Chernoguzov, D. Lucchetti, N. C. Brown, T. M. Gatterman, S. K. Halit, K. Gilmore, J. A. Gerber, B. Neyenhuis, D. Hayes, and R. P. Stutz, Realization of real-time fault-tolerant quantum error correction, Phys. Rev. X **11**, 041058 (2021).

[14] P. O. Schmidt, T. Rosenband, C. Langer, W. M. Itano, J. C. Bergquist, and D. J. Wineland, Spectroscopy using quantum logic, Science **309**, 749 (2005).

[15] S. A. King, L. J. Spieß, P. Micke, A. Wilzewski, T. Leopold, E. Benkler, R. Lange, N. Huntemann, A. Surzhykov, V. A. Yerokhin, J. R. C. López-Urrutia, and P. O. Schmidt, An optical atomic clock based on a highly charged ion, Nature (London) **611**, 43 (2022).

[16] N. Schwegler, D. Holzapfel, M. Stadler, A. Mitjans, I. Sergachev, J. P. Home, and D. Kienzler, Trapping and ground-state cooling of a single H_2^+, Phys. Rev. Lett. **131**, 133003 (2023).

[17] J. M. Cornejo, R. Lehnert, M. Niemann, J. Mielke, T. Meiners, A. Bautista-Salvador, M. Schulte, D. Nitzschke, M. J. Borchert, K. Hammerer, S. Ulmer, and C. Ospelkaus, Quantum logic inspired techniques for spacetime-symmetry tests with (anti-)protons, New J. Phys. **23**, 073045 (2021).

[18] M. A. Rowe, A. Ben-Kish, B. Demarco, D. Leibfried, V. Meyer, J. Beall, J. Britton, J. Hughes, W. M. Itano, B. Jelenkovic *et al.*, Transport of quantum states and separation of ions in a dual RF ion trap, arXiv:quant-ph/0205094.

[19] D. Leibfried, E. Knill, C. Ospelkaus, and D. J. Wineland, Transport quantum logic gates for trapped ions, Phys. Rev. A **76**, 032324 (2007).

[20] R. Bowler, J. Gaebler, Y. Lin, T. R. Tan, D. Hanneke, J. D. Jost, J. P. Home, D. Leibfried, and D. J. Wineland, Coherent diabatic ion transport and separation in a multizone trap array, Phys. Rev. Lett. **109**, 080502 (2012).

[21] A. Walther, F. Ziesel, T. Ruster, S. T. Dawkins, K. Ott, M. Hettrich, K. Singer, F. Schmidt-Kaler, and U. Poschinger, Controlling fast transport of cold trapped ions, Phys. Rev. Lett. **109**, 080501 (2012).

[22] T. Ruster, C. Warschburger, H. Kaufmann, C. T. Schmiegelow, A. Walther, M. Hettrich, A. Pfister, V. Kaushal, F. Schmidt-Kaler, and U. G. Poschinger, Experimental realization of fast ion separation in segmented Paul traps, Phys. Rev. A **90**, 033410 (2014).

[23] H. Kaufmann, T. Ruster, C. Schmiegelow, F. Schmidt-Kaler, and U. Poschinger, Dynamics and control of fast ion crystal splitting in segmented Paul traps, New J. Phys. **16**, 073012 (2014).

[24] L. E. de Clercq, H.-Y. Lo, M. Marinelli, D. Nadlinger, R. Oswald, V. Negnevitsky, D. Kienzler, B. Keitch, and J. P. Home, Parallel transport quantum logic gates with trapped ions, Phys. Rev. Lett. **116**, 080502 (2016).

[25] J. D. Sterk, H. Coakley, J. Goldberg, V. Hietala, J. Lechtenberg, H. McGuinness, D. McMurtrey, L. P. Parazzoli, J. Van Der Wall, and D. Stick, Closed-loop optimization of fast trapped-ion shuttling with sub-quanta excitation, npj Quantum Inf. **8**, 68 (2022).

[26] H. N. Tinkey, C. R. Clark, B. C. Sawyer, and K. R. Brown, Transport-enabled entangling gate for trapped ions, Phys. Rev. Lett. **128**, 050502 (2022).

[27] T. Meiners, J.-A. Coenders, J. Mielke, M. Niemann, J. Cornejo, S. Ulmer, and C. Ospelkaus, Fast adiabatic transport of single laser-cooled $^9Be^+$ ions in a cryogenic Penning trap stack, arXiv:2309.06776.

[28] D. Hanneke, J. Home, J. D. Jost, J. M. Amini, D. Leibfried, and D. J. Wineland, Realization of a programmable two-qubit quantum processor, Nat. Phys. **6**, 13 (2010).

[29] V. Negnevitsky, M. Marinelli, K. K. Mehta, H.-Y. Lo, C. Flühmann, and J. P. Home, Repeated multi-qubit readout and feedback with a mixed-species trapped-ion register, Nature (London) **563**, 527 (2018).

[30] K. Sosnova, A. Carter, and C. Monroe, Character of motional modes for entanglement and sympathetic cooling of mixed-species trapped-ion chains, Phys. Rev. A **103**, 012610 (2021).

[31] W. C. Burton, B. Estey, I. M. Hoffman, A. R. Perry, C. Volin, and G. Price, Transport of multispecies ion crystals through a junction in a radio-frequency Paul trap, Phys. Rev. Lett. **130**, 173202 (2023).

[32] S. A. Moses, C. H. Baldwin, M. S. Allman, R. Ancona, L. Ascarrunz, C. Barnes, J. Bartolotta, B. Bjork, P. Blanchard, M. Bohn, J. G. Bohnet, N. C. Brown, N. Q. Burdick, W. C. Burton, S. L. Campbell, J. P. Campora, C. Carron, J. Chambers, J. W. Chan, Y. H. Chen *et al.*, A race-track trapped-ion quantum processor, Phys. Rev. X **13**, 041052 (2023).

[33] J. P. Home, Quantum science and metrology with mixed-species ion chains, in *Advances In Atomic, Molecular, and Optical Physics*, edited by E. Arimondo, P. R. Berman, and C. C. Lin (Academic Press, San Diego, 2013), Vol. 62, pp. 231–277.

[34] D. Kienzler, Quantum harmonic oscillator state synthesis by reservoir engineering, Ph.D. thesis, ETH Zurich, 2015.

[35] See Supplemental Material at http://link.aps.org/supplemental/10.1103/PhysRevResearch.6.L032059 for a detailed description of the fitting model for the extraction of the phonon population, the micromotion compensation procedure, the temporal shape of the applied trap voltages, results on the separation of single-species crystals, a comparison of separation excitation for Be-Ca and Ca-Be, and the separation of larger ion crystals. It also contains Refs. [22,24,33,34,39,45,46].

[36] J. P. Home and A. M. Steane, Electrode configurations for fast separation of trapped ions, Quantum Inf. Comput. **6**, 289 (2006).

[37] R. Lechner, C. Maier, C. Hempel, P. Jurcevic, B. P. Lanyon, T. Monz, M. Brownnutt, R. Blatt, and C. F. Roos,

[38] Y. Lin, J. P. Gaebler, T. R. Tan, R. Bowler, J. D. Jost, D. Leibfried, and D. J. Wineland, Sympathetic electromagnetically-induced-transparency laser cooling of motional modes in an ion chain, Phys. Rev. Lett. **110**, 153002 (2013).

[39] V. Negnevitsky, Feedback-stabilised quantum states in a mixed-species ion system, Ph.D. thesis, ETH Zurich, 2018.

[40] M. Marinelli, Quantum information processing with mixed-species ion crystals, Ph.D. thesis, ETH Zurich, 2020.

[41] R. B. Blakestad, C. Ospelkaus, A. P. VanDevender, J. H. Wesenberg, M. J. Biercuk, D. Leibfried, and D. J. Wineland, Near-ground-state transport of trapped-ion qubits through a multidimensional array, Phys. Rev. A **84**, 032314 (2011).

[42] O. V. Ivakhnenko, S. N. Shevchenko, and F. Nori, Nonadiabatic Landau-Zener-Stückelberg–Majorana transitions, dynamics, and interference, Phys. Rep. **995**, 1 (2023).

[43] X. Chen, A. Ruschhaupt, S. Schmidt, A. del Campo, D. Guéry-Odelin, and J. G. Muga, Fast optimal frictionless atom cooling in harmonic traps: Shortcut to adiabaticity, Phys. Rev. Lett. **104**, 063002 (2010).

[44] J. D. Jost, J. P. Home, J. M. Amini, D. Hanneke, R. Ozeri, C. Langer, J. J. Bollinger, D. Leibfried, and D. J. Wineland, Entangled mechanical oscillators, Nature (London) **459**, 683 (2009).

[45] Y. Ibaraki, U. Tanaka, and S. Urabe, Detection of parametric resonance of trapped ions for micromotion compensation, Appl. Phys. B **105**, 219 (2011).

[46] C. Mordini, F. Lancellotti, V. Negnevitsky, M. Marinelli, R. Oswald, and T. Saegesser, PYTRANS (2023), https://doi.org/10.5281/zenodo.10204606.